Investigation of $Si_{1-x}Ge_x$ ($x \geq 0.85$) Solar Cells for Affordable High Efficiency Solar Energy Conversion

Thesis

Presented in Partial Fulfillment of the Requirements for a Bachelor's of Science in Chemical Engineering with Honor's Research Distinction in Electrical and Computer Engineering

By

Deep B. Shah

The Ohio State University

2015

Dissertation Committee:

Steven A. Ringel, Advisor

Tyler J. Grassman

Copyright by

Deep B. Shah

2015

Abstract

Increasing global demand on energy mixed with climate change is demanding a cleaner, more robust energy source. Moreover, access to low cost energy sources in much of the developing world is essential to sustain human vitality and growth. Thus, solar photovoltaics has come to the forefront of the clean energy realm as one of the most promising energy generation devices. The novel semiconductor material known as $Si_{0.05}Ge_{0.95}$ has been proposed as an ideal bottom cell (infrared sensitive) as part of a multijunction stack that has the potential to exceed 45% energy conversion efficiency in a low cost format. However, these devices have not been studied experimentally; therefore the devices must be experimentally investigated and the cells' dependence on material properties and processing must be determined and an optimized process flow must be developed. This has been done via various processing techniques and electrical characterization tools such as lighted current-voltage, quantum efficiency (QE), and energy-dispersive X-ray spectroscopy (EDX), as part of a Department of Energy supported effort. A working device has been produced using a Ni/Ge/Au front contact, which have made ohmic contact to the material without spiking through the junction. An internal quantum efficiency (IQE) measurement greater than 50% within the 1000 – 1600 nm wavelength range has also been measured on the cell. The information obtained thus far has created a pathway forward to substantially increase the IQE within the cell, making it amenable for future integration into a final multijunction solar cell architecture that has a practically achievable efficiency limit of 45%-50%.

Dedication

This document is dedicated to my family, friends, and mentors.

Acknowledgments

First off, I thank Dr. Steve Ringel for allowing me to work on this project. If it was for him allowing me to join his group at the end of my freshman year, I am not so sure that I would be pursuing a research career now. His knowledge of the subject matter and his mentoring has been invaluable.

I thank Dr. Tyler Grassman for helping me over the past few years with this project and with others. He has taught me a great deal about semiconductor physics, and that has really helped to spark my interest in the area. I also thank him for taking the time to serve on my thesis committee.

I thank Dr. John Carlin for meeting with me on countless occasions to go over to processing and device fabrication. Without his help, I would not have a working device, as he also helped process some of the devices.

I thank Chris Ratcliff, or the now Dr. Chris Ratcliff, and Dan Chmielewski for teaching me how to use much of the equipment at Nanotech West and within CL360. Their patience and teaching was incredibly valuable when I was starting out and now.

I thank Dr. Santino Carnevale and Dr. Drew Cardwell for the various discussions about life as a PhD student to device physics. These conversations allowed me to learn so much more about life after undergrad, and helped me decide to choose to pursue a PhD.

Additionally, thank you to Dr. Eugene Fitzgerald and his group at MIT, without them, I would not have any samples to process or characterize.

Finally, thank you to the staff at Nanotech West. Without them, I would have not accomplished my processing as I did not know how to work any of those tools.

Vita

May 2011 .....Troy High School

May 2015 .....B.S. Chemical and Biomolecular Engineering, The Ohio State University

Publications

Conference Proceedings:

1) T.J. Grassman, D.B. Shah, J.A. Carlin, and S.A. Ringel, "Exploration of epitaxial quantum dots within wide bandgap metamorphic host materials for intermediate band solar cells", IEEE 2013 PVSC, 284-287 (2013).
2) D. Shah, P. Patel, P. Kudo, A. Steinberg, and W. Herold, "Feasibility of rainwater harvesting on Scott Laboratory", IEEE 2013 GHTC, 361-364 (2013).

Presented at Conferences:

3) D. Shah, T.J. Grassman, J.A. Carlin, E.A. Fitzgerald, and S.A. Ringel "Investigation of $Si_{0.05}Ge_{0.95}$ Solar Cells for Affordable High Efficiency Solar Energy Conversion", Denman Undergraduate Research Forum, (2015).

Fields of Study

Major Field: Chemical and Biomolecular Engineering

Minor Field: Economics

Table of Contents

List of Figures

Preface

This work was not done independently. Many along the way helped with epitaxial growth, processing, and characterization. Doctoral students within Dr. Eugene Fitzgerald's group at MIT did all of the material growths within their chemical vapor deposition chamber. Dr. Tyler Grassman created the device structure designs that were sent to MIT to be grown. Additionally, Dr. John Carlin assisted in processing; he processed various samples within Generation I, II, and III in addition to the samples the author of this work processed. SIMS analysis was done at NREL. Finally, Dr. Santino Carnevale carried out the EDX measurements.

Chapter 1: Introduction

1.1 Motivation

Current energy consumption in the world is higher now than it has ever been and that trend is projected to rise. However, the majority of grid scale energy across the world relies on fossil fuels, such as coal and natural gas, which produce greenhouse gases such as carbon dioxide. The Intergovernmental Panel on Climate Change states that in order to avoid mass catastrophe for life, the average global temperature rise has to be limited to 2 ^{o}C when compared to pre-industrial temperatures [1]. Additionally, society is moving ever closer to that 2 ^{o}C cap as the current average global temperature rise is 0.8 ^{o}C [2]. In order to avert the temperature rise, fossil fuels need to be consumed less, and one study reports that in order to meet the 2 ^{o}C goal, a third of all oil reserves, half of all natural gas reserves, and 80% of all the current coal reserves should remain unused and underground [3]. Thus, in order to compensate for the unburnable carbon, solar energy has come to the forefront in disrupting the traditional energy mix. Currently, solar energy supplies approximately 1% of the total energy generated, but by 2035, solar energy is expected to produce 16% of the total electricity the world demands [4]. In order to make this feasible, much effort has been applied to research and development of better performing solar cells than the traditional, single junction silicon devices.

Conventional solar cells with a single bandgap have a theoretical maximum efficiency of 33.7% at an ideal bandgap energy of 1.34 eV [5]. However, due to economic and scalability reasons, Si is typically used to fabricate photovoltaics, whose maximum theoretical efficiency is 29% due to its non-ideal bandgap of 1.1 eV and recombination issues [5]. Due to low theoretical efficiencies for these single p-n junction (single bandgap) cells, so-called multijunction (MJ) photovoltaics are being studied to harness a greater portion of the solar spectrum more efficiently [6]. In this regard, SiGe has been suggested as an ideal semiconductor with which to create a lower bandgap "bottom cell" within certain MJ stacks. In particular, high Ge content ([Ge]≥85%) SiGe alloys are of primary interest for triple and quad junction cells due to its near ideal bandgap in order to act as an infrared "scavenging" device. A large challenge, however, is to grow $Si_{0.05/0.15}Ge_{0.95/0.85}$ with a low threading dislocation density (TDD), that are naturally present in these $Si_{0.05/0.15}Ge_{0.95/0.85}$ alloys. Dislocations are created since the $Si_{0.05/0.15}Ge_{0.95/0.85}$ crystalline layers must be grown on a Si substrate, which creates a mismatch in the equilibrium lattice constants between $Si_{0.05/0.15}Ge_{0.95/0.85}$ and Si that is relieved by the creation of dislocation defects. High TDD leads to lower photovoltaic material quality, which drastically diminishes the maximum power point, and must be maintained to an acceptably low concentration.

In addition, n-type SiGe is difficult to make ohmic contact to due to Fermi-level pinning near the valence band [7]. Due to the Fermi-level pinning in Ge rich n-type SiGe, high levels of doping are needed to achieve ohmic contacts. Non-ohmic contacts cause large resistances at the surface; thus the number of carriers that can be collected is

dramatically reduced. This can reduce the maximum power the cell is able to generate. Metal spiking, which causes device shortages, is another known issue for SiGe.

Figure 1 shows the bandgap vs. lattice constant for SiGe along with the other materials that have been proposed to be a part of a III-V/Si MJ stack [6]. If the project is successful, then MJ photovoltaics can be developed whose total efficiency is greater than 45%.

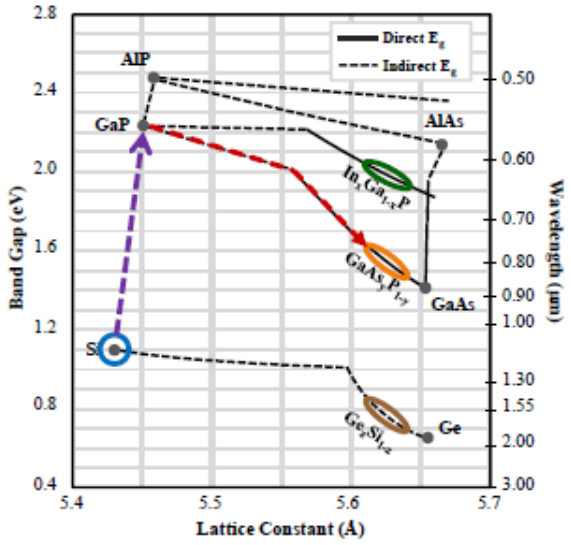

Figure 1: Bandgap vs lattice constant for proposed SiGe subcell [6]

1.2 Objectives

The aim of this research project was to identify ohmic contacts for the SiGe subcell, to design a highly efficient SiGe photovoltaic device, and to characterize and understand the electronic properties of these novel materials.

1.3 Thesis Organization

This thesis is the culmination of research conducted over 2013-2015 academic years along with the summer of 2014 and 2015. The thesis is organized as follows:

- Chapter 2 will cover basic solar cell physics along with solar cell design and bandgap engineering.
- Chapter 3 will cover how the SiGe cells were processed and prepared into photovoltaic devices along with the characterization techniques.
- Chapter 4 delves into the experimental results and the discussion of those results.
- Chapter 5 provides a summary and conclusion of the work along with ideas for future work.

Chapter 2: Background

2.1 Basics of Solar Cell Physics

Solar cells are diodes that can convert solar energy into usable, electrical energy. As they are typically semiconductor devices, it is necessary to understand the theory of solar cells, and this following section will cover the basics of doping, carrier generation and recombination, along with the p-n junction.

2.1.1 Doping

All semiconductors have a bandgap (E_g). The bandgap is separated into a valence band and a conduction band, which arises due to quantum mechanical interactions from a periodic material structure. The conduction band, with minimum energy E_c (i.e. conduction band edge), is the higher of the two bands and it houses excited electrons. The excited electrons leave behind gaps in the valence band (E_v) which can be referred to as holes, or "positive electrons." The space between the conduction band and valence band is considered the forbidden energy zone due to energy quantization, thus, electrons can only move from the valence band to the conduction band. Additionally, within the forbidden zone in semiconductors, there is an energy level known as the Fermi level. The Fermi level is when the probability of an electron occupying a space within the valance or conduction band is equal to ½.

Within an intrinsic semiconductor, at any temperature above 0 K, a portion of the electrons reside in the conduction band. This is because statistically, there are a few electrons that have enough energy to be excited into the conduction band. Within an

intrinsic semiconductor, the concentration of electrons, *n*, in the conduction band is equal to the concentration of holes, *p*, within the valence band. Therefore, the intrinsic Fermi level lies exactly midway between the valence and conduction bands. The carriers, the electrons and holes, allows the semiconductor to conduct electricity. However, within a solar cell, the intrinsic carrier concentration is not generally enough.

In order to improve upon electrical conduction, impurities, also known as dopants, are generally added into the semiconductor. The dopants can be either n-type or p-type, where the n-type introduces an excess of electron carriers within the conduction band and the p-type introduces an excess of holes within the valence band.

Typical n-type doping for Si or Ge would be phosphorous, arsenic, or antimony, which are all group V elements [8]. An n-type semiconductor introduces an impurity such that the atom has an extra valence electron when compared to the bulk, pure material. This in turn allows the extra electron to be energized very easily and sent into the conduction band. Thus, in an n-type material, the electron is the majority carrier and the hole is the minority carrier. Additionally, in an n-type semiconductor, the Fermi level shifts up from its intrinsic value due to an increased number of electrons in the conduction band, and this can be seen in Figure 2.

P-type dopants include group III atoms such as boron, aluminum, gallium, and indium for Si or Ge [9]. A p-type dopant introduces an impurity to an intrinsic semiconductor such that the atom has one fewer electron in its valence orbital, thus creating a “hole” within the valence band. This hole is what allows conduction, as electrons can move from space to space. In a p-type semiconductor, the Fermi level shifts

down from its intrinsic value due to the increased number of holes in the valence band, and this can be seen in Figure 2.

Figure 2: Diagrams of the energy band containing the intrinsic Fermi levels along with representations for a) an n-type semiconductor and b) a p-type semiconductor[10]

2.1.2 Generation

In order for a solar cell to generate energy, it needs to absorb photons to produce carriers that can supply energy to an external load. Photovoltaic devices can only absorb photons whose energy is at or above their bandgap energy, and any wavelength below that energy will pass through the material. If the energy of the incoming photon is far greater than the E_g of the material, then an electron will be energized far into the conduction band, but will then thermalize down to E_c, thus losing some energy as heat.

Generally, the absorption of photons increases with increasing energy above E_g, and those with higher energy tend to be absorbed near the surface of the material. However, excessive absorption of energy well above the E_g will cause excessive heating of the material along with wasted energy, as that thermalized heat cannot be recovered. A trade-

off must be done when determining which material to use as a solar cell to ensure good absorption, but also maintaining a high energy output.

Additionally, there are two types of bandgaps, an indirect gap and a direct gap. An indirect gap material, like SiGe, means that in the energy, E, vs crystal momentum, k, diagram, the valence band peak is offset in k-space when compared to the conduction band minimum. Therefore, in order for a carrier to be excited into the conduction band, both a photon and phonon need to be absorbed simultaneously, which is quantum mechanically not favorable. This leads to low absorption coefficients. Whereas a direct gap solar cell's conduction and valence bands match up, meaning the material only needs to absorb a photon. This leads to large absorption coefficients for the material. The energy-momentum diagram for indirect and direct gap semiconductors can be seen in Figure 3.

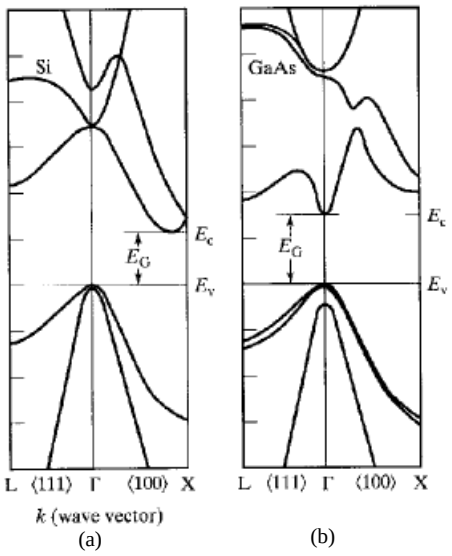

Figure 3: E-k diagrams of a) an indirect bandgap and b) a direct bandgap [10]

2.1.3 Recombination

There are two main types of carrier recombination that occur in semiconductors: radiative recombination and non-radiative recombination.

Radiative recombination is when an excited electron in the conduction band relaxes back to the valence band to recombine with a hole by emitting a photon with a wavelength similar to the E_g. Because the emitted photon is close to the bandgap, the photon will have a very low absorption coefficient and will most likely not be reabsorbed by the material, however, photon-recycling can occur within the material. Radiative recombination is the major form of recombination within direct gap materials.

Auger recombination describes the recombination process through three carriers. An electron from the conduction band recombines to with a hole while simultaneously transferring its energy to another electron within the conduction band. This highly energized electron then thermalizes down to the edge of conduction band and gives off the excess energy as heat. Auger recombination is the main form of recombination in indirect gap semiconductors and in materials that are very highly doped.

Shockley-Read-Hall (SRH) recombination only occurs in materials that have defects (eg. all real-life materials). These defects introduce energy states within the forbidden zone that are called traps. These traps can then capture carriers, electrons and holes, which then allow them to recombine. SRH recombination is very prevalent in materials with multiple defects, which leads to the great care that is taken when growing solar cells

that are lattice matched with low TDD. This will be briefly touched on later in this chapter.

Additionally, within a solar cell, there are major issues with recombination at the surface of the material. At the surface, it can be imagined that the material has many "dangling" bonds which facilitate the recombination of carriers. Additional impurities at the surface also introduce mid-gap states which promote carrier recombination rates.

2.1.4 The p-n Junction

The p-n junction is the basis for crystalline solar cells. A p-n junction is the interface between the p-type material and the n-type material. A depletion region is created at the interface between a p- and n- type material due to the diffusion of carriers into either material. Electrons diffuse towards the p-type side while holes diffuse towards the n-type side in order to establish equilibrium. Once equilibrium is reached, an internal electric field is created at the interface due to charge separation, hence why the depletion region is also known as the space charge region.

Under illumination, carriers are excited in either the p- or n- type materials and have a lifetime equal to the average minority carrier lifetime. If the minority carriers (electrons in p-type, holes in n-type) make it to the junction, then they are swept across the junction where they become the majority carrier, thus spatially separating the holes and electrons. Figure 4 is a representation of a p-n junction.

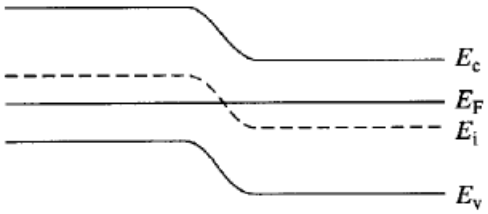

Figure 4: Band diagram for a p-n junction [10]

As is seen in the representation, when a p-n junction is created, the Fermi levels within the p- and n- type materials align. This causes band bending, where carrier electrons move down in energy in the conduction band and carrier holes move up in energy in the valence band. The depletion region is the area where the bands bend.

2.2 Solar Cell Design

Within a solar cell, there are four main portions to a single junction solar cell, and those are the base, emitter, window/passivation layers and contacts. A representation of the cross section of a solar cell can be seen in Figure 5.

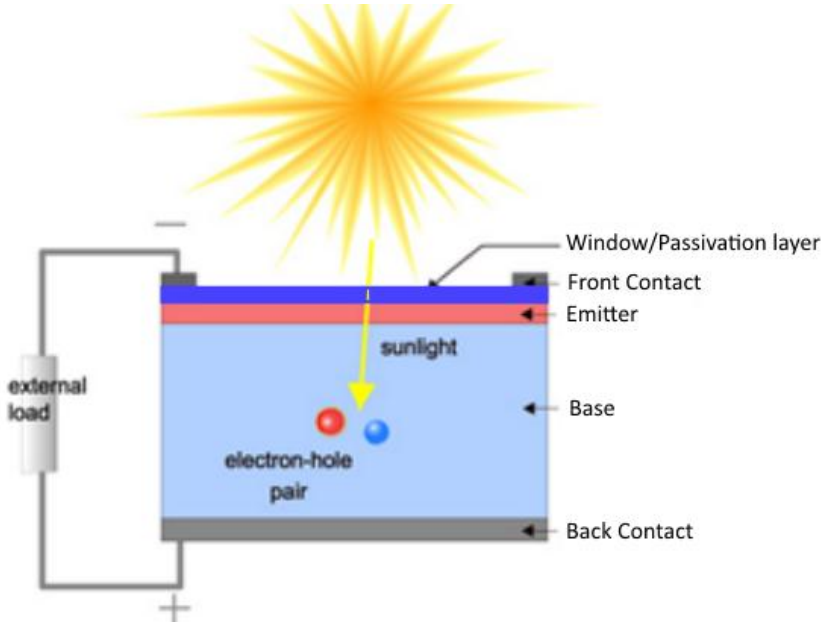

Figure 5: Cross section of a generic solar cell [11]

The base of the solar cell is doped as either n- or p-type, so long as the doping is of a different type than the emitter. For the case of SiGe, the base is generally p-type because electron carriers within SiGe tend to have longer lifetimes than holes, therefore the electron minority carriers in the p-type base have a higher probability of reaching the depletion region [12]. The emitter for SiGe solar cells tends to be n-type and thin. High energy photons have a higher probability of being absorbed within the emitter. The thin emitter provides a higher likelihood of collecting the minority carrier.

In order to mitigate what would normally be a high intrinsic front surface recombination velocity, a passivating layer is generally grown on top of the emitter. This passivating layer is also known as the "window layer" because it is typically of a much higher bandgap than the emitter directly below. The purpose of the window/passivating layer is to decrease the front surface recombination velocity. Additionally, there are issues with carrier recombining in the rear surface, so a back surface field (BSF), which is a highly doped portion in the base, is used to deflect minority carriers back towards the junction.

Finally, photovoltaics require a method to transfer the internal carriers that are generated to the external load. This is accomplished through the utilization of metallic contacts. These contacts need to be ohmic (i.e. non-rectifying) with low contact resistances such that there are not efficiency losses within the cell. In order to achieve ohmic contacts on high Ge content n-type SiGe, extremely high levels of doping are required. High levels of n-type doping are required to avoid Fermi level pinning in the SiGe material [13].

2.3 Bandgap Engineering

In order to design multijunction solar cells, some band engineering must be done. Figure 1 is a diagram of the bandgap of materials to their lattice constants. This figure helps to portray that in order to a solar cell to have a certain E_g, the material composition must be engineered. In order to achieve a certain E_g, the material composition is altered, which then changes the lattice constant. In order to construct MJ photovoltaics, the various cells must be lattice matched, or grown using buffer layers in order to remove some of the strain that could cause large amounts of defects within the material which could act as recombination centers [14].

The purpose of the remainder of the thesis is to discuss the processing that was necessitated in order to construct working SiGe photovoltaics, the characterization tools that were utilized and to delve into the results from the characterization.

Chapter 3: Processing & Characterization

The SiGe wafers were grown at MIT in Prof. Eugene Fitzgerald's group using chemical vapor deposition. Growth structure diagrams were sent to MIT for them to grow, and the grown materials were then shipped back to OSU to process and characterize.

3.1 Processing

Photovoltaic processing contains three main steps, and those are photolithography, metal contacting, and device isolation. Each one of these steps must be carried out within a cleanroom in order to minimize the number of foreign particles interact with the surface of the SiGe material.

Each SiGe wafer went through similar processing steps, which will be outlined in this section. The SiGe was grown on a p-type Si substrate, thus aluminum was to be used as the backside contact [15]. In order to do so, the front side was protected by spin-coating SPR220 with an approximate thickness of 10 μm. Afterwards, the substrate was dipped in diluted hydrofluoric acid (1:200 by volume, HF:H_2O) in order remove the SiO_2 on the backside as well as to passivate the back surface. The HF:H_2O acid dip allows for ohmic contact formation onto the p-type Si [16]. After the oxide etch, the substrate is placed into an evaporator in order to deposit aluminum. Once the Al is deposited onto the backside, the photoresist is cleaned off, and the substrate is annealed at 400 ^{o}C for 5 minutes, which allows an Al-Si layer to form at the interface, thus creating ohmic contact with the material.

The front side of a photovoltaic device is neatly patterned with metal so as to allow enough incident light to pass through to the device. In order to pattern the device, SPR220 is spin-coated onto the surface, and a mask is then used to expose UV radiation to certain sections. Figure 6 below displays the front side patterning before metal deposition. Once the photoresist (PR) has been exposed to UV radiation, MF-319, a developer solution, is used to remove the portions of PR that was not exposed to the UV light. Once again, the substrate is submerged in an acid dip, HF:H_2O for SiGe, in order to remove the native oxide and to help passivate the surface [16]. The real challenge for the n-type SiGe has been to determine a metal that allows for ohmic contact formation, which will be covered in the results and discussion sections. After the metal deposition step, the remaining PR is removed from the surface of the substrate using acetone, methanol, and isopropanol.

Finally, the devices are isolated from one another by etching through the window, the emitter, and the base. This is done using a plasma ICP with CF_4 as the etching gas. The isolation allows each of the individual cells to be characterized.

3.2 Characterization

Characterization of the fabricated devices was done using a plethora of tools. 4-point probe measurements were carried out on devices in order to determine if the metal contacts were ohmic or rectifying and to determine the contact resistance. The 4-point probe was used on circular transmission line measurement (CTLM) devices on the SiGe substrate. Both internal and external quantum efficiency (IQE and EQE) measurements were carried out in order to determine the ratio between the number of carriers collected

by the cell to the number of photons incident to the cell. IQE gives the ratio with the sample reflectance removed from the calculation while EQE is the ratio including reflection. Therefore, EQE is always lower than IQE due to some sample reflection. An ideal cell would have a square quantum efficiency curve at unity, signifying that all the photons absorbed above the bandgap produce minority carriers that are collected. A real cell will have reduced IQE/EQE at high energy and near bandgap energy photons. The IQE/EQE will be lower at high energy photons because the absorption of those photons is very high and will be absorbed close to the surface of the cell. Absorption near the front of the cell leads to recombination of the carriers due to a high recombination velocity at the surface. A lower surface recombination velocity of the emitter can be achieved if a good window layer is applied, however the surface can still impact cell performance. Low energy photons right above the bandgap will also have lower IQE/EQE due to low absorption coefficients at those wavelengths. Therefore, the photons will produce minority carriers further into the cell. If the photon is absorbed deep into the cell, then the excited carriers can have a lower likelihood of collection because the minority carrier's lifetime can be less than what the carrier requires to be collected at the junction. Other characterization was also done outside of OSU, such as secondary ion mass spectroscopy (SIMS) and transmission electron microscopy (TEM). SIMS is used to check doping levels within the material whereas TEM is used to determine the physical integrity of the material, such as the number of defects.

PC1D is a device simulation code that can be found online. It is a very accurate modeling tool for fairly simple solar cells, and thus it was also used in order to simulate

the quantum efficiencies of the materials before they were grown. As the wafers were not grown at OSU, PC1D was used to design potential cells, and the growths were then compared to the PC1D model. Parameters were then adjusted in the PC1D model in order to match the measured quantum efficiency, and these parameters included doping and minority carrier lifetime.

Chapter 4: Experimental Results & Discussion

The extent of this research occurred in three generations. Three different designs were grown in Dr. Fitzgerald's group, and the second and third generations were iterations to the first and second, respectively, based on recommendations from characterization.

4.1 Generation I

Generation I came with two samples, however, one was not characterized because the emitter was doped incorrectly. The other sample was used, and the structure can be seen in Figure 6.

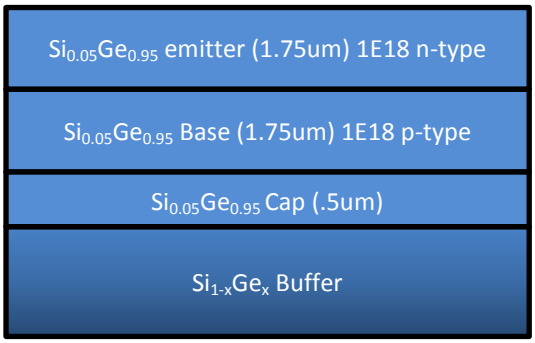

Figure 6: Material design for the Generation I solar cell

The cell was processed with the backside contact being aluminum and the front side contact as nickel/germanium/gold. The measured quantum efficiency of the cell can be seen in Figure 7.

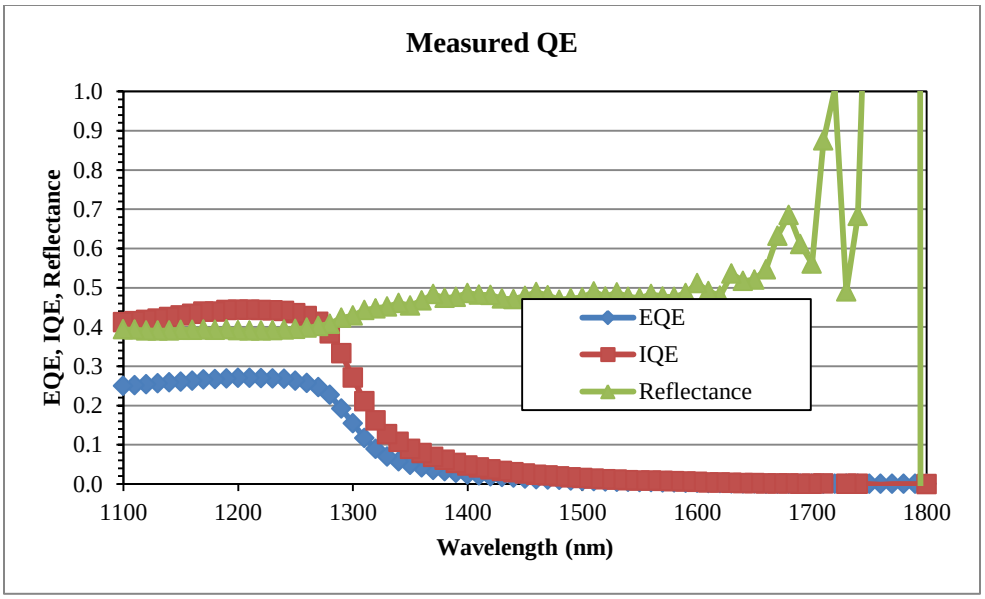

Figure 7: Quantum efficiency measurement for the first generation sample

This generation of cells did not contain a front surface passivation layer or a BSF. It can be seen that the IQE was limited to below 50%. A simulation was run in PC1D in order to match the characteristics of the sample, and the results are displayed in Figure 8. Reflection data was used from the measured sample for the simulation.

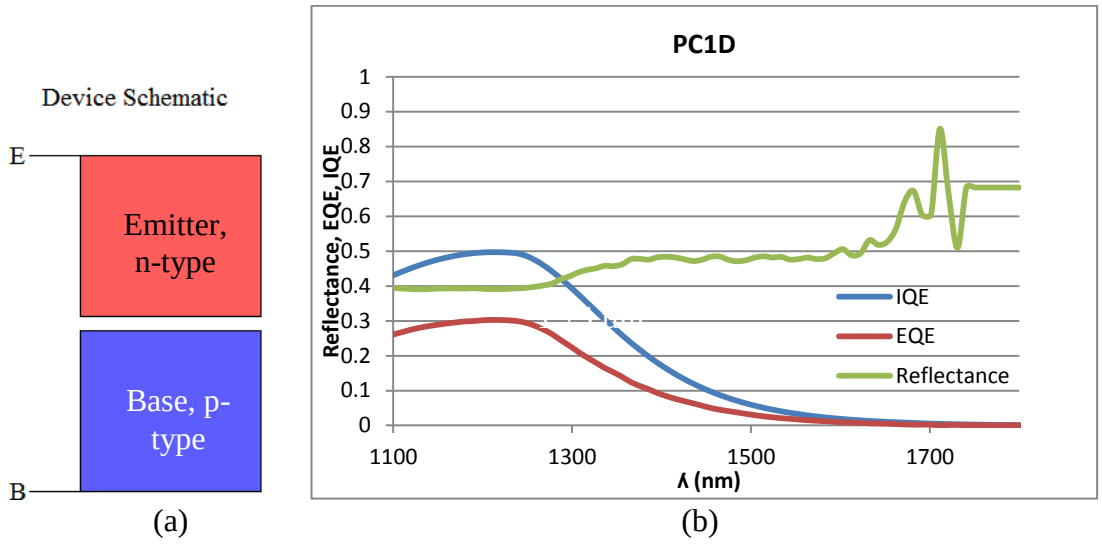

Figure 8: PC1D modeling of the first generation cell, (a)the device schematic, and (b) the simulated QE

As can be seen in the model, it matches the measured values relatively well. The IQE is limited to below 50%, however, the drop off beyond 1300 nm is not quite as steep. The simulation was modeled by assuming a front and rear surface recombination rate of $1x10^{7}$ cm/s. The lifetime of the minority carriers was adjusted, but the values did not play a major role in the outcome of the simulation, so the minority carrier lifetime was assumed to be 1 µs. Some papers report hole and electron carrier lifetimes in Si to be around10^{-6} s at a temperature of 300 K with doping levels at 10^{18} cm^{-3}, thus it was assumed to be a similar value for Ge [17].

SIMS data was collected for this sample, and it confirmed the existence of a p-n junction within the material. The results can be seen in Figure 9. The junction can be seen at 1.75 µm, which was the desired material design.

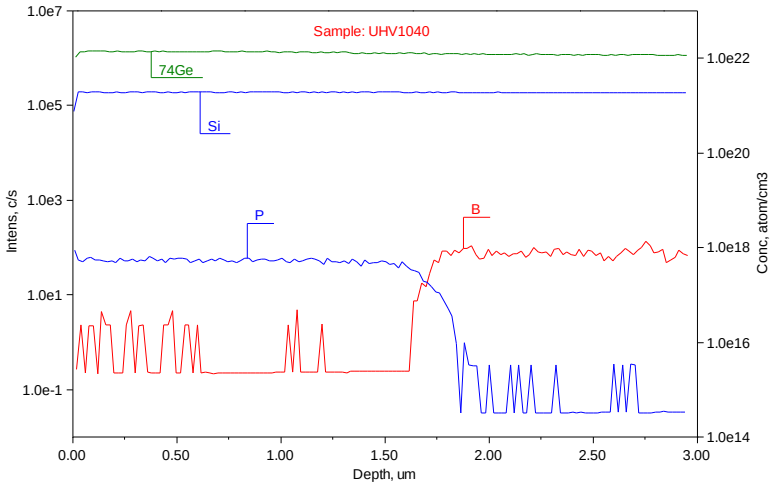

Figure 9: SIMS results for Gen I sample, phosphorus was used as the n-type dopant and boron as the p-type

From the first generation of devices, it was observed that the IQE was limited to 40-45% in the Si-filtered spectral range. This was most likely caused by the lack of a window/passivation layer and the lack of a BSF layer. Additionally, the emitter was not doped very heavily, which led to poor ohmic contacts on the front side and therefore, high contact resistances. These poor ohmic contacts were most likely due to Fermi level pinning on the front [13]. For the next iteration, these issues were noted and it was determined that a window layer needed to be included to help passivate the front surface along with a BSF to reflect minority carriers that could recombine at the back surface.

4.2 Generation II

Generation II was an improvement upon generation I. After recognizing the limitations on the previous substrate, a new material design was sent to Dr. Fitzgerald's

group in order to be grown in their CVD chamber. The second structure can be seen in Figure 10.

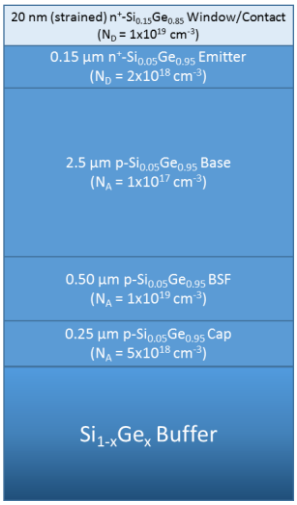

Figure 10: Generation II substrate design

The generation II design contains a BSF along with a window/contact layer to reduce recombination near the rear and the front of the cell, respectively. Additionally, TEM images were taken and the results showed that the window layer was strained but it did not generate additional defects. Also, the TDD levels were kept to ~$3x10^6$ cm^{-2}. The TEM images can be seen in Figure 11.

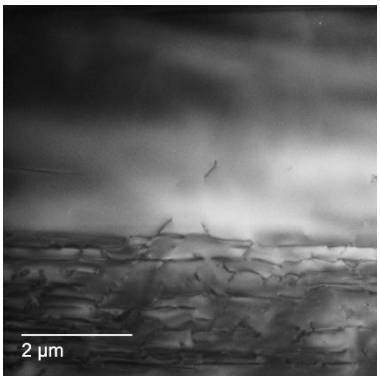

Figure 11: TEM images of the 2nd generation material

The SIMS data, which can be seen in Figure 12, suggests that target doping levels within the material were achieved, where the n-type doping was phosphorous, and the p-type doping was boron. The step increase in boron at ~2.7 µm is the BSF layer.

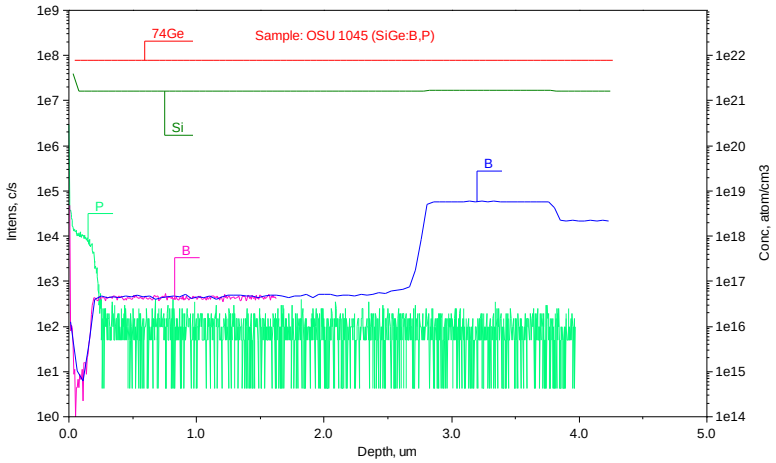

Figure 12: SIMS results for the second generation material

The sample was a double sided growth, meaning that it was grown symmetrically on both sides of the Si substrate (wafer). Thus, one side of the SiGe had to be etched away to

expose the Si substrate in order to facilitate good quality ohmic contact. However, when the substrate was etched, it led to cracking on the front surface (due to large strain build-up and catastrophic release in the SiGe buffer), which then led to metal spiking through the p-n junction. The spiking caused the cell to short circuit, and in order overcome this issue, front to front contacts were made on the surface of the material, eliminating the need to etch the back surface, but further complicating the analysis. Cracking of the material after the ICP etch can be seen in Figure 13.

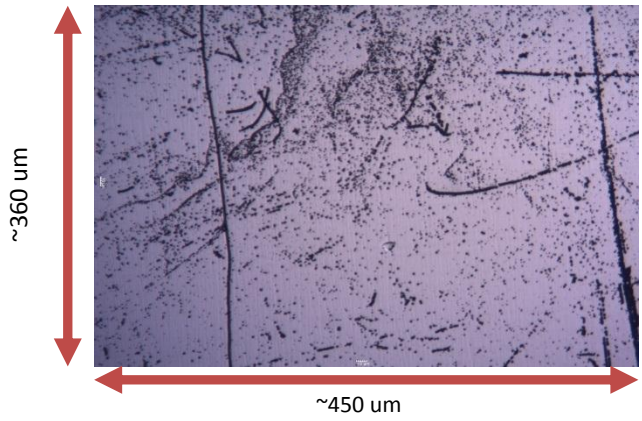

Figure 13: Cracking on the back of the wafer, not represented are similar cracks on the front surface

A few different metals were tried to create ohmic contact, such as Al and Ni/Ge/Au, and of those it was found that Ni/Ge/Au could create ohmic contact to the surface as long as the annealing temperature was kept low. The ohmic contact was determined by utilizing an IV scan. The QE of the device can be seen in Figure 14.

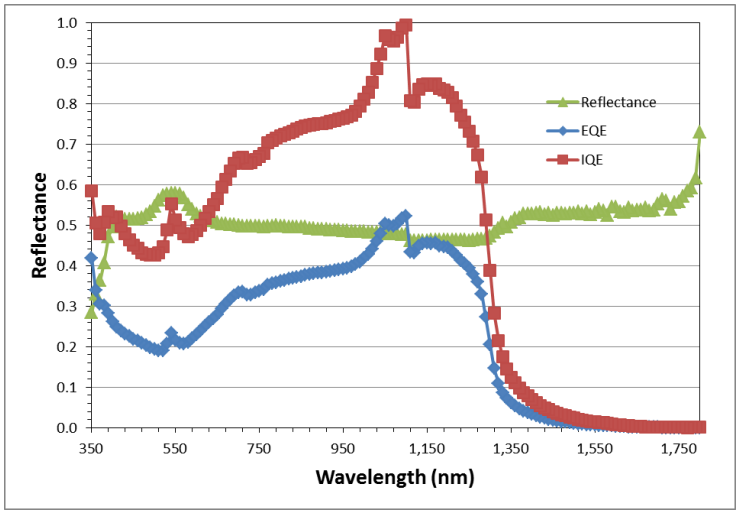

Figure 14: QE of the 2nd generation cell

It can be seen that there is a near step increase in reflection right around 1350 nm. It is suspected that the increase in reflection occurs because that is around the bandgap switch between direct gap and indirect gap. The direct gap wavelength is higher than that of the indirect gap, and after the transition, due to the lower absorption coefficients of the indirect gap, a larger portion of light is reflected back at the detector. This reflection could originate from the back contact along with the gold sample stage. While we do not know the origin of the odd features in the 300-1100 nm range, it is suspected that they may be related to the use of front to front contacts, or due to some unusual interfacial activity within the complex device structure. However, this behavior does not show up in the PC1D modeling that is shown in Figure 15.

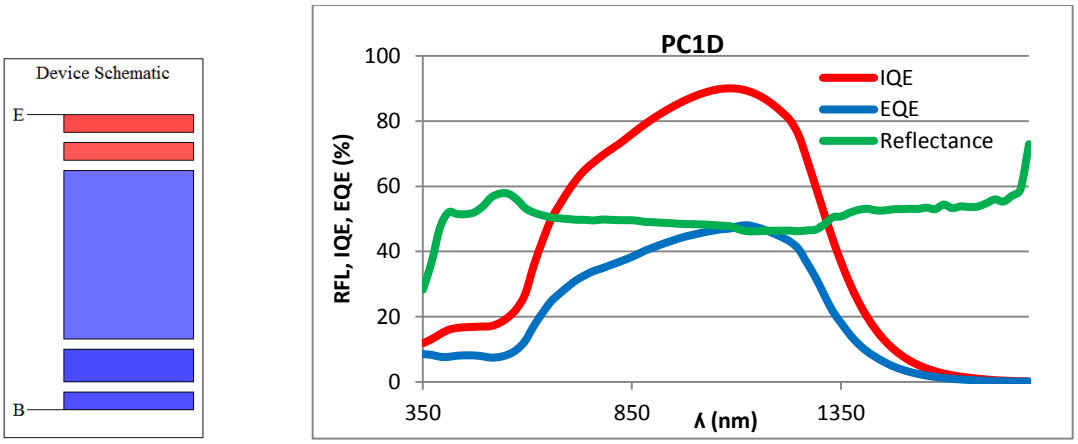

(a) (b)

Figure 15: PC1D modeling of the gen II device; (a) the device structure with 5 parts, (b) modeled QE

The device's structure in PC1D emulates the original design, in that the layers from top to bottom are: $Si_{0.15}Ge_{0.85}$ (n^+ doping, window/contact layer), $Si_{0.05}Ge_{0.95}$ (n doping, emitter), $Si_{0.05}Ge_{0.95}$ (p doping, base), $Si_{0.05}Ge_{0.95}$ (p^+ doping, BSF), and $Si_{0.05}Ge_{0.95}$ (p doping, back side cap). The front surface recombination was assumed to be $1x10^7$ cm/s for both types of carriers, and the minority carrier lifetime was assumed to 10^{-6} s.

Generation II was an improvement upon the first set of devices. The Si filtered IQE was much higher than generation I, however it can be seen that the IQE and EQE drop off rapidly beyond 1200 nm. The extreme drop in QE could be because the SiGe absorption went from direct band absorption to indirect band absorption. Indirect gap devices tend to have much smaller absorption coefficients, and that would explain the sudden loss in QE.

A highly doped, n-type $Si_{0.15}Ge_{0.85}$ window layer was added to the front of the material in order to assist in the creation of an ohmic contact to the device. However, as

the window layer was only 20 nm and the emitter was 150 nm, combined with the cracking of the front surface, it led to device shorting. Thus, in order to create ohmic contacts to the device, front to front surface contacts were made, where a diode structure near the solar cells was shorted in order to transfer current through the cell. These front to front contacts may have also increased contact resistance, which could have negatively impacted the device QE. The device cracking posed a major processing challenge, so for the next iteration, the backside growth was not included. This eliminated the need to do a backside etch prior to device fabrication and processing. Additionally, it was noted that the window or emitter layer needed to be thicker in order to prevent metal diffusion through the emitter and into the junction.

The cause of the strange behavior in the 350-1100 nm range has not yet been determined. There will be future work to help identify the cause of the discontinuities within the data.

4.2.1 Ohmic Contact Formation

Ohmic contact formation with the Generation II material was a large hurdle to obtaining working devices. The n-type contact, Ni/Ge/Au, seemed to penetrate through the junction and short the devices when annealed at the standard temperature of 390 ^{o}C for 30 seconds. Some research literature suggested that Ni would perform well as a ohmic contact to the n-type emitter [18]. Ni was attempted as the front contact, however, it was found that the devices were shorted, which was most likely caused by metal diffusion through the p-n junction. 25 nm of Ni was deposited onto the sample followed by 200 nm of Al. After the metal deposition, the metal was annealed at 340 ^{o}C. As can be seen by

Figure 16, the IV curve is almost completely linear between two front side diodes, thus indicating an electrical short.

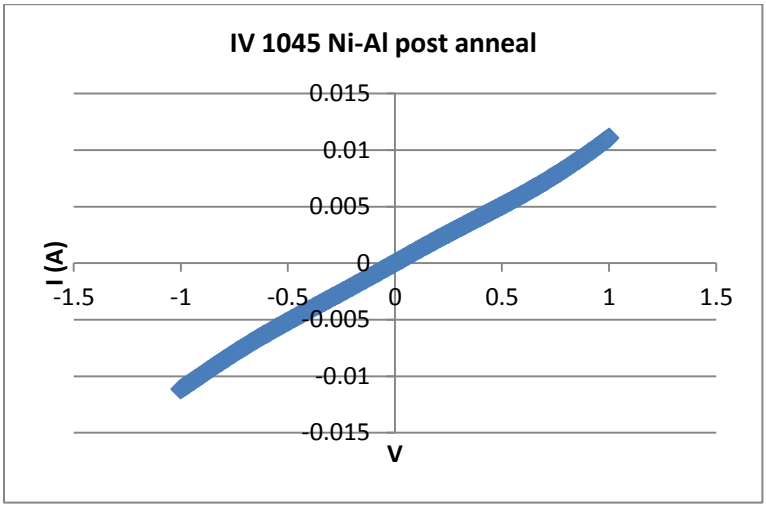

Figure 16: IV curve of a front to front diode measurement

In order to determine the diffusion depth, energy-dispersive X-ray spectroscopy (EDX) was attempted on a cross section of the sample. However, conclusive results from the sample could not be obtained due to sample charging and drifting within the sample, which lead to the sample shifting over time of the measurement. Additionally, due to the sample shifting, multiple data sets could not be collected and averaged as the averages tended to shift in relation to sample depth. Figure 17 shows data form the Ni/Al front contact along with the cross section of the sample from EDX.

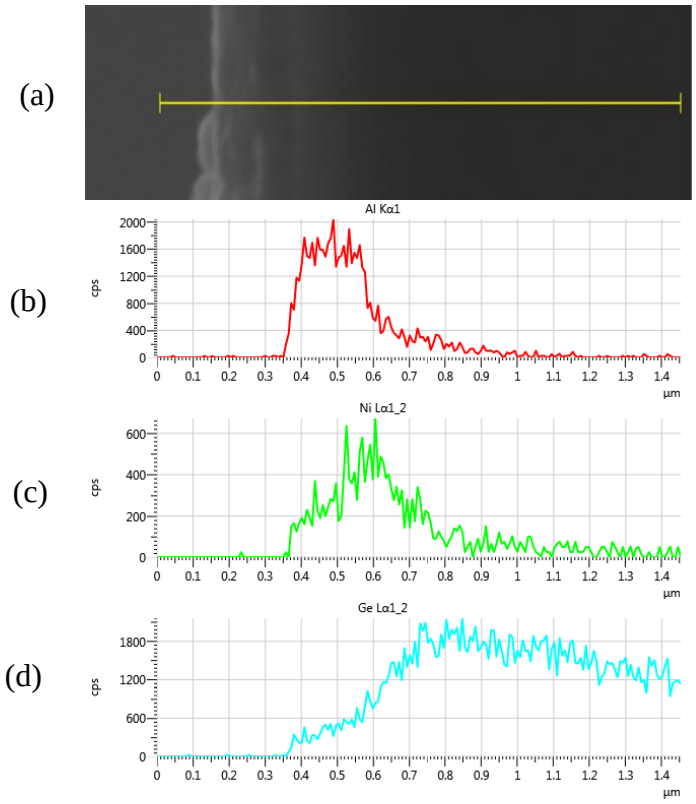

Figure 17: EDX data a) image of the cross-section of the sample, b) Al in relation to sample, b) Ni in relation to sample, and c) Ge in relation to sample

As can be seen in the figure, the far left line for Al is not an abrupt vertical line, as it should be, and this is due to the aforementioned charging and sample movement. While the results were not conclusive for metal diffusion, it is strongly suggested by the IV data, and cracking within the front surface promoted the problem. However, the challenge was overcome by utilizing a Ni/Ge/Au contact with an anneal temperature at 250 ^{o}C for 30 seconds as opposed to the standard 390 ^{o}C for 30 seconds.

4.3 Generation III

Generation III was both a side step and an improvement upon generation II. It was a sidestep in that the Ge content was lower than the previous two generations. This was because MIT had material for this structure around, and it was faster to ship these samples than to grow a 95% SiGe wafer. However, it was an improvement upon the two previous generations because it was a single sided epitaxial growth, which allowed for simpler processing. Additionally, the samples had a GaAsP window layer, which is much easier to make ohmic contact. The structures for the two designs can be seen in Figure 18.

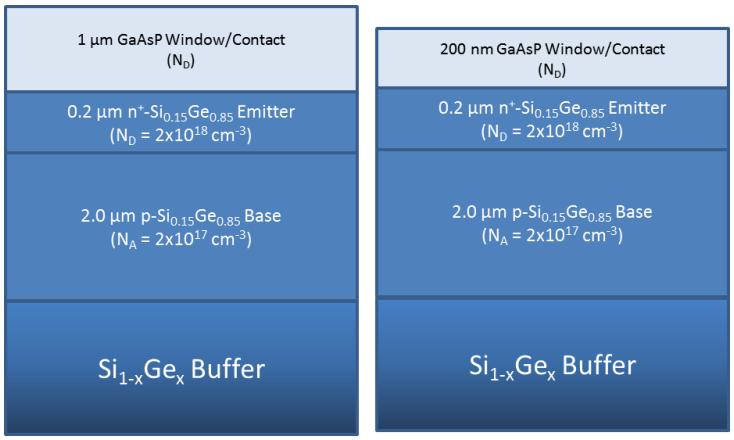

Figure 18: Generation III samples

While it is not evident from the figure, these samples did have a BSF layer, with the buffer layer acting simultaneously as the BSF. A set of samples were processed by Dr. Carlin, where the backside contact was aluminum, and the front side contact being the Ni/Ge/Au alloy. A quantum efficiency measurement of the thick window sample can be seen in Figure 19. Quantum efficiency measurements for the thin window sample could

not be done because there was no light response from the devices, which may indicate that the devices were shorted.

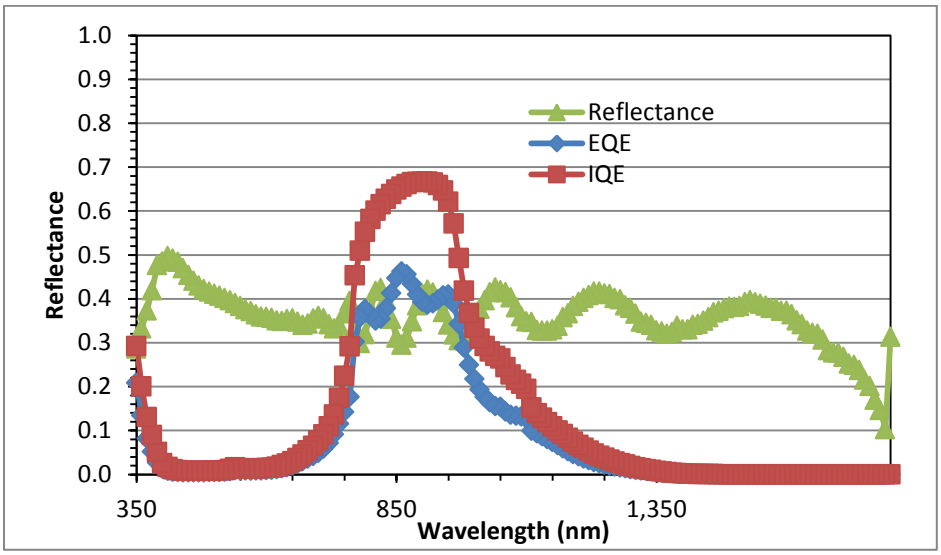

Figure 19: QE of the thick window device

It can be seen that the EQE is limited to below 50% while the IQE is less than 70%. Figure 20 is a model of the QE of the thick window device. The model was done on PC1D and the structure emulated the design that was shown in Figure 18.

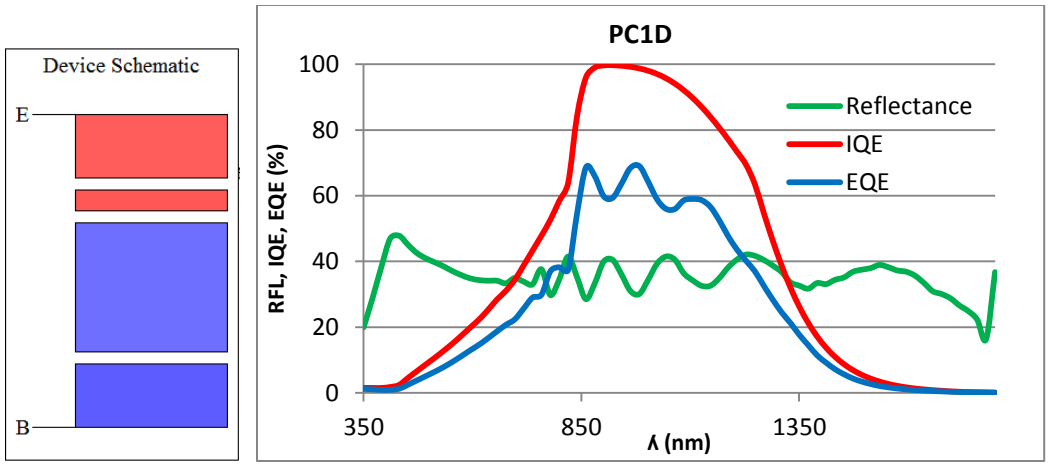

(a) (b)

Figure 20: PC1D modeling of the gen III device; (a) the thick window structure with 4 parts, (b) modeled QE

As can be seen by the PC1D simulation, the real device did not perform nearly as well. This could be because the device that was measured was a bad device, and there might be better devices on the material. However, additional devices were not measured at the time of this writing, and more will be measured in the future. The IQE might also be limited due to unknown defects or issues at the interface that were not characterized. The overall shape of the modeled device matches quite well with the collected data, however it is not quite up to the same performance.

Chapter 5: Conclusion

5.1 Summary & Conclusion

It was found that the Generation II devices were the best performing in terms of quantum efficiency. Generation III wafers are not fully ready for integration into a quadruple junction solar cell because their bandgap is too high. Generation III wafers absorb solar wavelengths that overlap strongly with Si, thus, Generation IV will have to be of a lower bandgap so it absorbs more of the Si filtered light.

Through the three generations of samples, a common trend was discerned. In order to maximize the quantum efficiency, device designs should include back surface fields, highly doped n-type emitters or window layers, and the CVD growth should be one sided in order to minimize front surface cracking. Additionally, a window layer should be included in order to reduce front side recombination velocities.

5.2 Future Work

There is much work still for this project. The future research entails obtaining another iteration of samples from Dr. Fitzgerald's group. A new set will be grown that has a thicker overall cell, an increase of 1.3 μm, which will improve upon absorption of longer wavelengths within the solar cell. Additionally, characterization such as QE and IV will be done in order to determine the electrical properties of the device. The new device should have better contacts, along with a BSF to help with carrier collections. Finally, if a good SiGe solar cell can be simulated, the cell will be wafer bonded to Si to prove that wafer bonding can be done while maintaining the integrity of the device.

References

[1] IPCC, 2014: Climate Change 2014: Mitigation of Climate Change. *Contribution of Working Group III to the Fifth Assessment Report of the Intergovernmental Panel on Climate Change*. Cambridge University Press, Cambridge, United Kingdom and New York, NY, USA.

[2] Schmunk, Robert B. *et al*. Five-Year Global Temperature Anomalies from 1880 to 2013. *NASA/Goddard Space Flight Center Scientific Visualization Studio*. (2014).

[3] McGlade, Christophe and Paul Ekins. The geographical distribution of fossil fuels unused when limiting global warming to 2 °C. *Nature* **517**, 187-190 (2015).

[4] IEA. Technology Roadmap: Solar Photovoltaic Energy, 2014 edition. *OECD/IEA*, (2014).

[5] Shockley, William and Hans J. Queisser. Detailed Balance Limit of Efficiency of p-n Junction Solar Cells. *Journal of Applied Physics* **32**, 510 (1961); doi: 10.1063/1.1736034.

[6] S.A. Ringel and J.A. Carlin. III-V/Active-Si Integration for Low-Cost High-Performance Concentrator Photovoltaics. *Funded by Dept. of Energy Sunshot Office under the Foundational Program to Accelerate Cell Efficiency (FPACE)*, (2011).

[7] Kasper, E., Oehm, M., and J. Lupaca-Schomber. High Ge content SiGe alloys: Doping and contact formation. *ECS Transactions* **16** (10) 893-904 (2008); doi: 10.1149/1.2986850.

[8] Brotzmann, Sergej and Hartmut Bracht. Intrinsic and extrinsic diffusion of phosphorus, arsenic, and antimony in germanium. *Journal of Applied Physics* **103**, 033508 (2008); doi: 10.1063/1.2837103.

[9] Chroneos, A. and H. Bracht. Diffusion of n-type dopants in germanium. *Journal of Applied Physics* **1**, 011301 (2014); doi: 10.1063/1.4838215.

[10] Pierret, Robert F. (1987). *Advanced Semiconductor Fundamentals*. Boston, MA: Addison-Wesley Longman Publishing Co., Inc.

[11] Honsberg, Christiana and Stuart Bowden. <http://pveducation.org/pvcdrom/solar-cell-operation/solar-cell-structure>. Accessed April 2015.

[12] Schaffler, F. et al. (2001). Properties of Advanced Semiconductor Materials GaN, AlN, InN, Bn, SiC, SiGe. New York, NY: John Wiley & Sons, Inc. 149-188.

[13] Kasper, E., Oehme, M., and J. Lupaca-Schomber. High Ge content SiGe alloys: Doping and contact formation. *ECS Transactions* **16**, (10) 893-904 (2008).

[14] Barrigon, E. et al. GaInP/GaInAs/Ge triple junction solar cells for ultra high concentration. *Proceedings of the 2009 Spanish Conference on Electron Devices,* (2009).

[15] Urrejola, Elias et al. Al-Si alloy formation in narrow p-type Si contact areas for rear passivated solar cells. *Journal of Applied Physics* **107**, 124516 (2010); doi: 10.1063/1.3437070.

[16] Yablonovitch, E. et al. Unusually Low Surface-Recombination Velocity on Silicon and Germanium Surfaces. *Physical Review Letters* **57**, 2 (1986).

[17] del Alamo, J.A. and R.M. Swanson. Measuring and modeling minority carrier transport in heavily doped silicon. *Solid State Electron* **30**, (11) 1127-1136 (1987).

[18] Gallacher, K. et al. Ohmic contacts to n-type germanium with low specific contact resistivity. *Applied Physics Letters* **100**, 022113 (1012); doi: 10.1063/1.3676667.